Journal Pre-proof

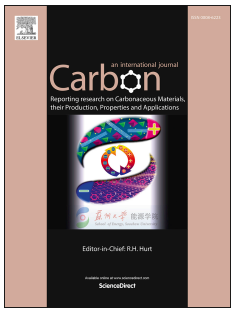

Nitrogen and Phosphorus Dual-doped Porous Carbons for High-Rate Potassium Ion Batteries

Xiaoqing Ma, Nan Xiao, Jian Xiao, Xuedan Song, Hongda Guo, Yongtao Wang, Shijia Zhao, Yiping Zhong, Jieshan Qiu

PII: S0008-6223(21)00398-5

DOI: https://doi.org/10.1016/j.carbon.2021.03.067

Reference: CARBON 16224

To appear in: *Carbon*

Received Date: 21 February 2021

Revised Date: 30 March 2021

Accepted Date: 31 March 2021

Please cite this article as: X. Ma, N. Xiao, J. Xiao, X. Song, H. Guo, Y. Wang, S. Zhao, Y. Zhong, J. Qiu, Nitrogen and Phosphorus Dual-doped Porous Carbons for High-Rate Potassium Ion Batteries, *Carbon*, https://doi.org/10.1016/j.carbon.2021.03.067.

Xiaoqing Ma: Methodology, Writing – Original Draft, Writing – Review & Editing.

Nan Xiao: Supervision, Conceptualization.

Jian Xiao: Formal analysis.

Xuedan Song: Theoretical calculations.

Hongda Guo: Resources.

Yongtao Wang: Resources.

Shijia Zhao: Resources.

Yiping Zhong: Theoretical calculations.

Jieshan Qiu: Supervision, Conceptualization.

Nitrogen and Phosphorus Dual-doped Porous Carbons for High-Rate Potassium Ion Batteries

Xiaoqing Ma[a], Nan Xiao[a,*], Jian Xiao[a], Xuedan Song[a], Hongda Guo[a], Yongtao Wang[a], Shijia Zhao[a], Yiping Zhong[a], Jieshan Qiu[a,b,*].

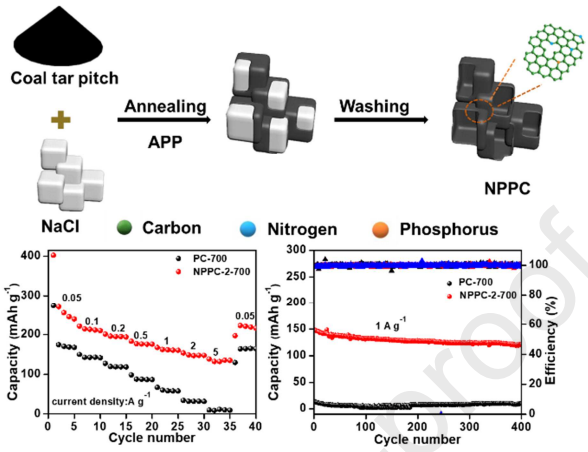

The nitrogen-phosphorus dual-doped porous carbon frameworks (NPPC) was successfully prepared by one-step carbonization. Due to the introduction of heteroatoms, the NPPC exhibits excellent rate capability and cycling stability.

Nitrogen and Phosphorus Dual-doped Porous Carbons for High-Rate Potassium Ion Batteries

Xiaoqing Ma[a], Nan Xiao[a,] *, Jian Xiao[a], Xuedan Song[a], Hongda Guo[a], Yongtao Wang[a], Shijia Zhao[a], Yiping Zhong[a], Jieshan Qiu[a,b,] *.

[a] State Key Lab of Fine Chemicals, School of Chemical Engineering, Liaoning Key Lab for Energy Materials and Chemical Engineering, Dalian University of Technology, Dalian 116024, Liaoning, China.

[b] College of Chemical Engineering, Beijing University of Chemical Technology, Beijing 100029, China.

*Corresponding authors. Tel:+86-411-84986024. E-mail addresses: nxiao@dlut.edu.cn (Nan Xiao), qiujs@mail.buct.edu.cn (Jieshan Qiu).

Abstract

Pitch-based porous carbons with the abundant resources and high conductivity have potential advantages as potassium-ion battery anode materials. However, they suffer from small interlayer distance and rare potassium storage sites. Herein, nitrogen and phosphorus dual-doped coal tar pitch-based porous carbons (NPPC) was prepared in one-step carbonization using ammonium polyphosphate as N and P source and studied as the anodes for the potassium ion batteries. NPPC delivers a high capacity retention of 81.8% over 400 cycles at 1.0 A g^{-1}. When the current density is raised to 10 A g^{-1}, it can still retain a reversible capacity of 126 mAh g^{-1}. The effects of carbonation temperature and ratio of ammonium polyphosphate to coal tar pitch on nitrogen and phosphorus doping contents were investigated by in situ Fourier transform infrared (FTIR) and synchronous thermal analysis. This work may shed light on the design of advanced potassium-ion battery by employing heteroatom doped functionalized soft carbons.

Keywords: potassium ion battery; in situ FTIR analysis; coal tar pitch; high rate; heteroatom doping.

1. Introduction

As the most successful commercial secondary battery, lithium-ion batteries are widely used in portable electronic devices and electric vehicles due to their high energy density and good cycle stability[1]. However, for the large-scale stationary energy storage like the grid, the cost is more important than the energy density. Due to the lack and uneven distribution of lithium resources, lithium prices are rising, which limits the application of lithium-ion batteries in the stationary energy storage [2-4]. Therefore, it is urgent to develop alternatives for LIBs based on earth-abundant metals. Along this line, potassium ion batteries (PIBs) have received more and more attention due to the abundant reserves of potassium (2.09 wt.%) in the Earth' s crust and the low negative redox potential of K/K^+ (-2.93 V) [5, 6]. However, the large radius (1.38 Å of K^+ compared to 0.76 Å of Li^+) results in sluggish diffusion kinetics of K^+, leading to a poor rate performance, which seriously slows down the development of PIBs.

Well-designed anode materials are crucial for boosting the rate performance of PIBs. In the past years, a mass of anode materials, which can be classified as alloying materials, conversion materials and intercalation materials, have been investigated and evaluated for PIBs [7, 8]. Among them, carbon materials[9-11], especially the heteroatom-doped carbons, have attracted the most attention of battery researchers because of their wide range of sources, low price and easy access [7]. Various dopant elements including N, S, B, and P have been proved to dramatically boost the electrochemical properties of carbons [12-14]. Among them, nitrogen, which could produce efficient defects and structural vacancies, as well as enhance the electronic conductivity of carbon materials, has been regarded as one of the most promising dopant for improving the potassium storage performance [15, 16]. Compared with

N, P has lower electronegativity and higher electron-donating ability. Therefore, the introduction of P atoms in carbon materials is expected to more significantly produce structural distortion and enhance electrochemical activity, which consequently accelerate the diffusion of ions and increase the reserves of potassium ions [17]. Previous works have demonstrated that co-doping of nitrogen and phosphorus can further improve the carbons' electrochemical performance due to the synergistic effect of N and P atoms [18, 19]. However, because of its large radius, the P content in N/P dual-doped carbons is usually quite low, which limits the full play of the synergistic effect [20]. In addition, the influencing factors on nitrogen and phosphorus co-doping are still not clear. Therefore, how to synthesize carbon material with suitable contents of nitrogen and phosphorus remains a big challenge.

In this work, we prepared N/P co-doped porous carbons (NPPC) by one-step carbonization using coal tar pitch (CTP) as carbon source, ammonium polyphosphate (APP) as N/P source and NaCl as template. Owing to the synergistic effect of nitrogen and phosphorus co-doping as well as porous structure, NPPC exhibits excellent rate performance (126 mAh g^{-1} at 10 A g^{-1}). The effect of heat treatment temperature and raw material composition on the N/P co-doping was investigated by in situ Fourier transform infrared (FTIR) spectroscopy and synchronous thermal analysis. This work promises a facile method of dual atomic doping for high rate PIBs.

2. Experimental section

2.1 *Preparation of NPPC*

Prior to the synthesis of NPPC, NaCl template with particle size of 5-8 μm was prepared by recrystallization as reported in our previous work [21]. In a typical run, 0.5 g CTP with soft point of 85 ^{o}C, 1.0 g APP and 5.0 g NaCl template were ground and mixed in agate mortar. The ground powder was heated at 280 ^{o}C for 2 h, and then carbonized at 600, 700 and 800 ^{o}C for 2 h in Ar with a heating rate of 5 ^{o}C/ min, and then washed with deionized water. The final products were named as NPPC-2-600, NPPC-2-700, NPPC-2-800. For comparison, the control samples were prepared under the same experimental conditions without the addition of APP and recorded as PC-700. And the sole N-doped porous carbon (NPC-700) was obtained by replacing APP with urea. To find the optimum ratio of CTP to APP, the samples with CTP and APP mass ratios of 1:1 and 1:3 were prepared at 700 ^{o}C, named as NPPC-1-700 and NPPC-3-700, respectively.

2.2 *Material characterization*

The morphology and nanostructure of the materials were observed by field emission scanning electron microscope (FESEM, FEI Nova Nano SEM 450). Transmission electron microscopy (TEM) images, selected area electron diffraction (SAED) and energy-dispersive X-ray spectroscopy (EDS) were made with transmission electron microscope (FEI Tecnai F20). The X-ray photoelectron spectroscope (XPS, Thermo ESCALAB 250) was used to analyze the elemental state of the materials. Thermogravimetry (TG) and differential thermal analysis (DTA) were conducted using a thermogravimetric analyzer (STA449F3 NETZSCH, Germany) from 25 to 900 □ under N_2 atmosphere at a heating rate of 10 ^{o}C min^{-1}. The gas products derived from pyrolysis of APP and CTP are analyzed by the in situ Fourier transform infrared spectroscopy (FTIR, Nicolet iS50). The X-ray diffraction (XRD) were

examined by Smart Lab 9 KW X-ray diffractometer with a Cu-Kα_1 source. Nitrogen adsorption/desorption measurements were obtained with a Micromeritics ASAP 2020 to measure pore structure. The density function theory and Brunauer-Emmett-Teller method were used to calculate pore size distribution and specific surface area, respectively.

2.3 *Electrochemical tests*

Electrochemical properties were measured using CR2016 coin-type cells, which were assembled in an Ar-filled glove box (O_2 < 0.1 ppm and H_2O < 0.1 ppm). The working electrodes were fabricated by mixing active material, carboxymethylcellulose and Super P with a weight ratio of 8:1:1 in deionized water to form a homogeneous slurry. The slurry was then coated on a Cu foil rapidly and dried at 80 ^oC for 12 h in vacuum. The mass loading of working electrode is about 1.0-1.4 mg/cm^2. The PIBs were assembled with K metal as the counter electrode, glass fiber (GF/C) as the separator, 0.8 mol L^{-1} KPF_6 dissolved in a 1:1 volumetric mixture of dimethyl carbonate and ethylene carbonate as the electrolyte. The galvanostatic discharge/charge tests were conducted within the voltage window of 0.01-3.0 V. The cyclic voltammetry (CV) measurements were performed within the voltage range of 0.01-3.0 V at various scan rates of 0.1-1.2 mV s^{-1}. The electrochemical impedance spectroscopy (EIS) test was performed over the frequency range of 100 kHz to 10 mHz.

2.3 *Calculation details*

All calculations were carried out on Vienna Ab initio Simulation Package using density functional theory (DFT) [22]. Generalized gradient approximation Perdew - Burke - Ernzerhof (GGA-PBE) method [23] and projector augmented wave (PAW) pseudopotential [24] calculations are adopted. Van der Waals interactions are considered using the DFT - D3

method [25, 26]. The cuto□ energy is set to 500 eV, and the Monkhorst - Pack mesh with 3×3×1 k point is applied for the Brillouin zone integration. The energy convergence criteria for electronic and ionic iterations were 10^{-4} eV and -0.05 eV/Å, respectively. The adsorption energy (ΔE_a) of K atom on the material was defined as follows: $\Delta E_a = E_{slab\text{-}K} - E_{slab} - E_K$, where $E_{slab\text{-}K}$ is the total energy of K atom adsorbed on slab, E_{slab} is the energy of slab, and E_K is the energy of K atom

3. Results and discussion

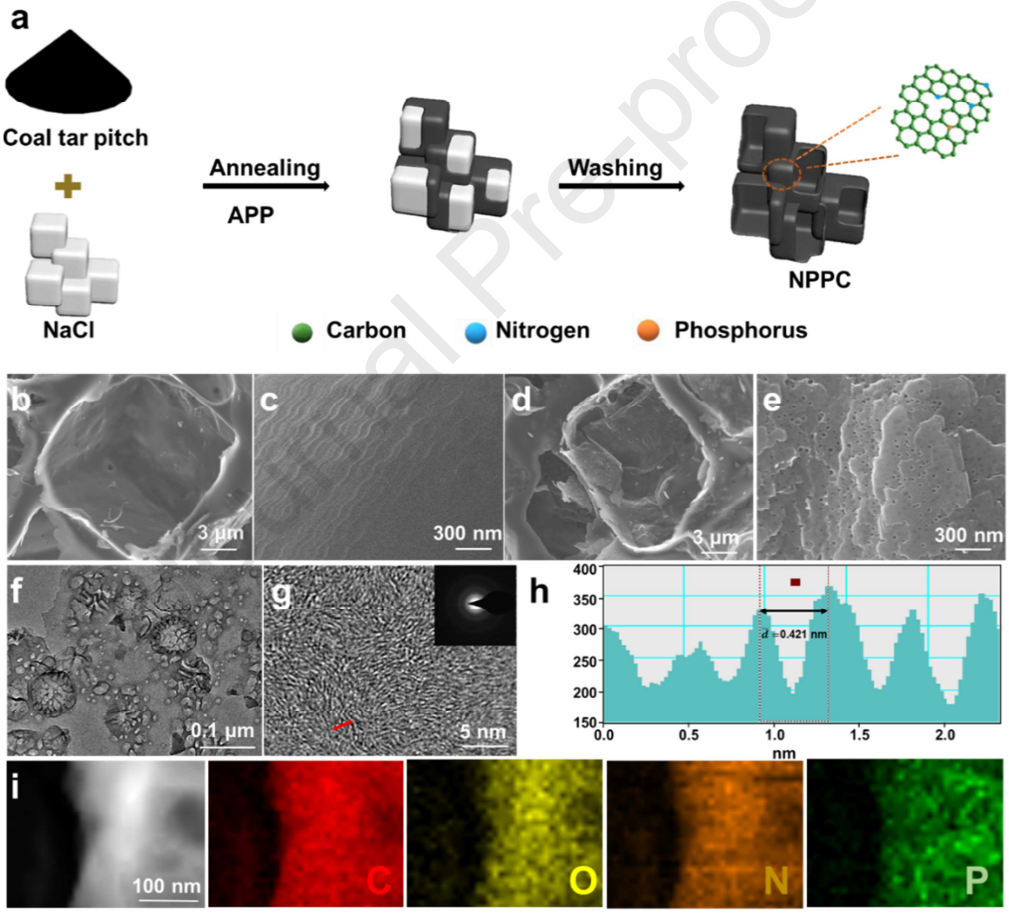

Fig. 1. (a) Schematic illustration for the synthesis of NPPC. (b) SEM and (c) high-magnification SEM images of PC-700. (d) SEM, (e) high-magnification SEM images, (f) TEM image and (g) HRTEM image with SAED pattern of NPPC-2-700. (h) average interspaces of NPPC-2-700 calculated by TEM diffraction fringe. (i) A typical TEM image

and the corresponding element mapping of NPPC-2-700 with carbon, oxygen, nitrogen, and phosphorous.

The schematic illustration for the synthesis of NPPC is shown in Fig. 1a. As shown in Fig. 1b and d, due to the addition of NaCl template, both the PC-700 and NPPC-2-700 possess a porous structure with pore size of 2 to 8 μm, which consist of cross-linked micron sheets. This structure is conducive to improving the electrochemical properties of the material [27, 28]. Different from the smooth surface of PC-700 (Fig. 1c), a large number of 10-30 nm mesopores (Fig. 1e) are found on the walls of NPPC-2-700, which is attributed to the decomposition of APP. TEM image further confirms such cross-linked micro-sized sheets accompanied with mesopore distribution (Fig. 1f). The porous structure with large surface area makes sure that electrolyte and electrode are in full contact which can shorten the ion diffusion distance. HR-TEM image (Fig. 1g) shows that NPPC-2-700 exhibits short range ordered carbon layer with interlayer spacing of 0.421 nm (Fig. 1h). The SAED image display diffused rings, demonstrating the amorphous nature of NPPC-2-700. The EDS mapping images (Fig. 1i) reveal homogeneous distribution of C, O, N and P among the NPPC-2-700, suggesting successful uniform doping of N and P.

From the analyses of XRD patterns (Fig. 2a), it is clear that all the three samples of PC-700, NPC-700 and NPPC-2-700 possess two broad peaks at around 21° and 43°, corresponding to the (002) and (100) crystal planes, respectively. Compared with PC-700, the (002) diffraction peaks of NPC-700 and NPPC-2-700 shift to a lower diffraction angle. According to Bragg equation, the average interlayer spacing (d_{002}) of NPC-700 and NPPC-2-700 are 0.409 and 0.416 nm respectively, which are larger than that of PC-700 (0.405 nm), suggesting that the

interlayer space of carbon materials can be expanded by the addition of urea or APP. Two obvious characteristic peaks are revealed by the Raman spectra of NPPC-2-700, NPC-700 and PC-700 (Fig. 2b), indexing to D band (1360 cm^{-1}) and G band (1580 cm^{-1}). The I_D/I_G ratio is usually used to qualitatively represent the disorder or the defects of carbon materials. Obviously, the I_D/I_G of NPC-700 (0.95) and NPPC-2-700 (0.99) are higher than that of PC-700 (0.81), due to the emerged defects by doping N and P heteroatoms.

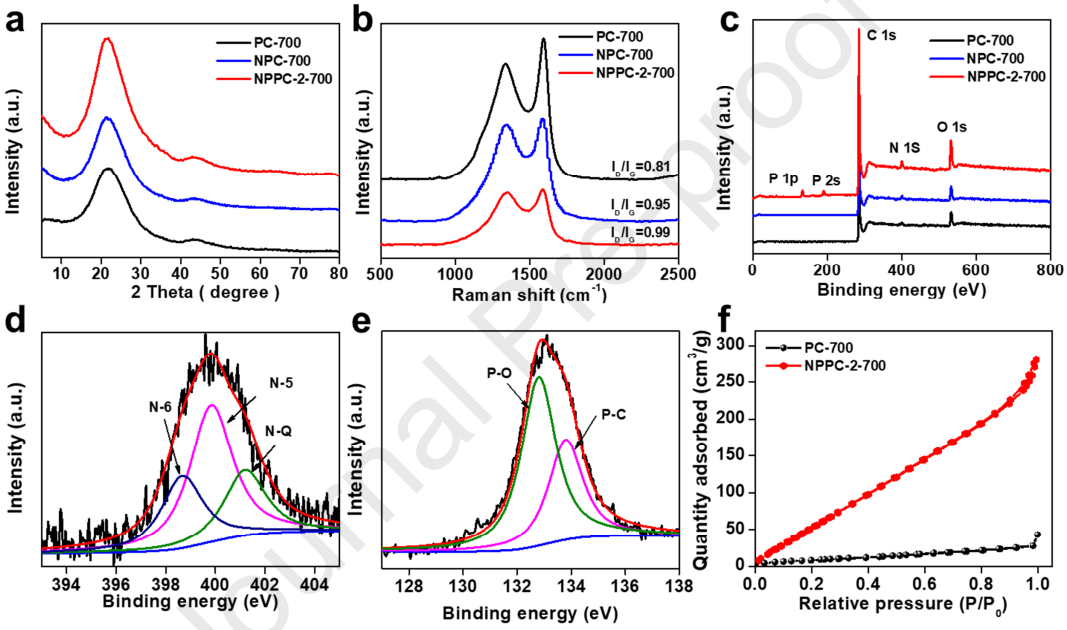

Fig. 2. XRD patterns (a), Raman spectra (b) and XPS survey spectra (c) of PC-700, NPC-700 and NPPC-2-700. N 1s spectrum (d), P 2p spectrum (e) of NPPC-2-700 . Nitrogen adsorption-desorption isotherms (f) of PC-700 and NPPC-2-700.

The state and contents of N and P in PC-700, NPC-700 and NPPC-2-700 were analyzed by XPS (Fig. 2c). The N and P contents of NPPC-2-700 are 3.68 at.% and 3.15 at.%, respectively (Table S1).The peaks located at 284.8, 286.2 and 287.7 eV (Fig. S1) belong to C-C, C-O/C-P and C=O/C=N bonding [18, 29], respectively, suggesting the successful doping of N and P.

The N 1s peaks of the NPPC-2-700 (Fig. 2d) can be deconvoluted into N-6 (398.7 eV), N-5 (399.8 eV) and N-Q (401.2 eV) [30, 31]. Similarly, the P 2p of the NPPC-2-700 (Fig. 2e) can be fitted into two peaks, responding to P-O (132.8 eV) and P-C (133.8 eV) [32, 33]. As shown in Fig. S2a, the contents of N-6 and N-5 in NPPC-2-700 are 26.0% and 50.5%, respectively. While the contents of P-O and P-C in NPPC-2-700 (Fig. S2b) are 63.0% and 37.0%, respectively. The N-6 and N-5 can provide active sites for potassium ion storage by introducing defects [4, 34]. The P-C bond is longer than the C-C bond, so P doping will cause the structure distortion of hexagonal carbon skeleton and increase the interlayer spacing [29]. At the same time, the electron donor capacity of phosphorus is higher than that of nitrogen, and the high content of phosphorus doping is expected to improve the conductivity of the carbons [33, 35, 36]. Additionally, the high oxygen content of carbon is also beneficial for the improvement of electrochemical properties of materials [33, 37].

The pore structure of PC-700 and NPPC-2-700 was investigated by nitrogen adsorption and desorption isotherm, as shown in Fig. 2f. PC-700 shows a quite small specific surface area of 33 $m^2 g^{-1}$ and pore volume of 0.069 $m^3 g^{-1}$. However, those of the NPPC-2-700 are increased to 332 $m^2 g^{-1}$ and 0.422 $m^3 g^{-1}$. The enlarged specific surface area can be attributed to the addition of APP, which releases NH_3 and H_3PO_4 at high temperature, and subsequently etch the pitch derived carbon to form pores. As exhibits in Fig. S3, the pore size distribution curve of NPPC-2-700 is centered at 5.08 nm. The mesoporous structure of NPPC-2-700 could shorten the diffusion path of ions and thus improve the rate performance of materials [37].

The PC-700 and NPPC-2-700 were used as anodes to assemble potassium half-cell for testing their electrochemical performance. As shown in Fig. S4a and Fig. 3a, the CV curves of

PC-700 and NPPC-2-700 appear a cathodic peak near 0.5 V in the first lap, which disappear in the subsequent laps and can be attributed to the formation a solid electrolyte interface (SEI) film. From the second circle, the CV curves are almost overlapped, indicating the good cycling stability of the samples. Fig. 3b and Fig. S4b represent the charge-discharge profiles of NPPC-2-700 and PC-700. At current density of 50 mA g^{-1}, the initial coulombic efficiency (ICE) of the NPPC-2-700 and PC-700 are 60.04% and 70.78%, respectively. The irreversible capacity can be mainly ascribed to the formation of SEI film [38], which is consistent with CV curves. The ICE of NPPC-2-700 is lower than that of PC-700 due to its higher specific surface area. Although the low ICE may have some adverse effects in practical application, the high specific surface area is crucial for improving the rate performance of electrode materials.

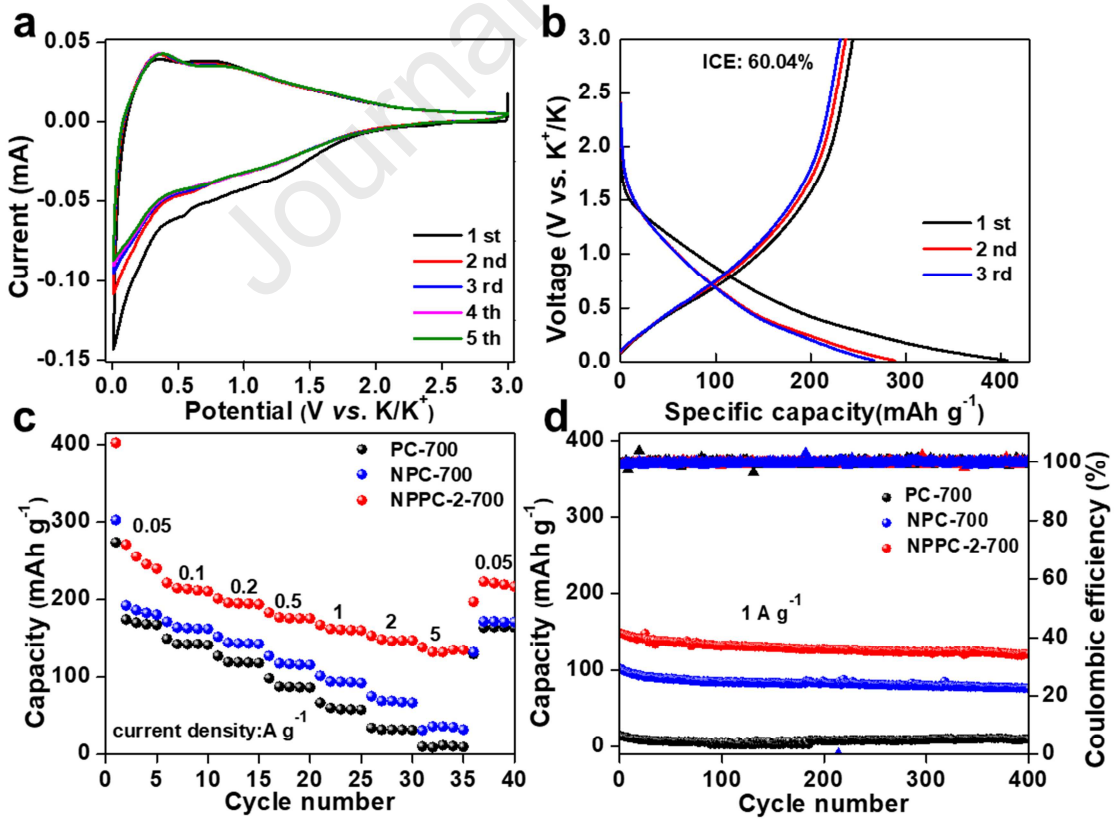

Fig. 3. (a) CV curves and (b) Charge-discharge profiles of NPPC-2-700. (c) Rate performance and (d) Long cycling performance of PC-700, NPC-700 and NPPC-2-700

When served as the working electrode of PIBs, NPPC-2-700 shows an initial charging specific capacity of 301 mAh g^{-1} at a current density of 25 mA g^{-1} (Fig. S5), which is higher than that of graphite (279 mAh g^{-1})[16]. Fig. 3c describes the rate capabilities of PC-700, NPC-700 and NPPC-2-700. The specific capacities of NPPC-2-700 and NPC-700 at each current density is higher than that of PC-700, indicating the positive role played by the N and P doping in the potassium storage. The NPPC-2-700 electrode shows discharge capacities of 240, 210, 194, 176, 160, 147 and 133 mAh g^{-1} at 0.05, 0.1, 0.2, 0.5, 1, 2 and 5 A g^{-1}, respectively, which is higher than that of NPC-700. The superior rate performance of the NPPC-2-700 compared with NPC-700 can be attributed to the high-level phosphorus doping which can enhance the carbons' interlayer spacing as well as electronic conductivity, and thus improving the kinetics of ion diffusion and electron transfer [19]. Even at a high current density of 1 A g^{-1}, the NPPC has an initial specific capacity of 170 mAh g^{-1}. After 400 cycles, the capacity retention rate of NPPC-2-700 is 81.8%, indicating the good cycle stability of NPPC-2-700 (Fig. 3d).

Electrochemical impedance spectroscopy analysis on fresh electrodes was carried out to explore the reasons why NPPC-2-700 shows excellent electrochemical properties. Fig. 4a represents Nyquist plots of PC-700, NPC-700 and NPPC-2-700, which consist of semicircle and sloping line. The semicircle in the high frequency region represents the charge transfer resistance, and the sloping line in the low frequency region represents the ion diffusion resistance. According to the equivalent circuit (inset of Fig. 4a), the charge transfer

208 resistances (R_{ct}) of PC-700, NPC-700 and NPPC-2-700 are 395.9, 1078.0 and 620.7 Ω,
209 respectively, as shown in Table S2. As a soft carbon, the coal tar pitch derived carbons
210 possess good electrical conductivity. While, the introduction of nitrogen and phosphorus will
211 produce defects and pores, as well as disordered microstructure, which results in the decrease
212 in conductivity[39].

213 The potassium diffusion coefficient can be calculated according to the following formula
214 [40]:

215 $$D = \frac{R^2T^2}{2A^2n^4F^4C^2\sigma^2} \quad (1)$$

216 In this formula, R is the gas constant, T is the absolute temperature, A is the surface area of
217 electrode sheets, n is the number of electrons transferred in electrochemical reactions, F is the
218 Faraday's constant, σ is the Warburg coefficient which is the slope of the linear relationship
219 between Z′ and $\omega^{-1/2}$ in the low frequency region of the impedance spectrum.

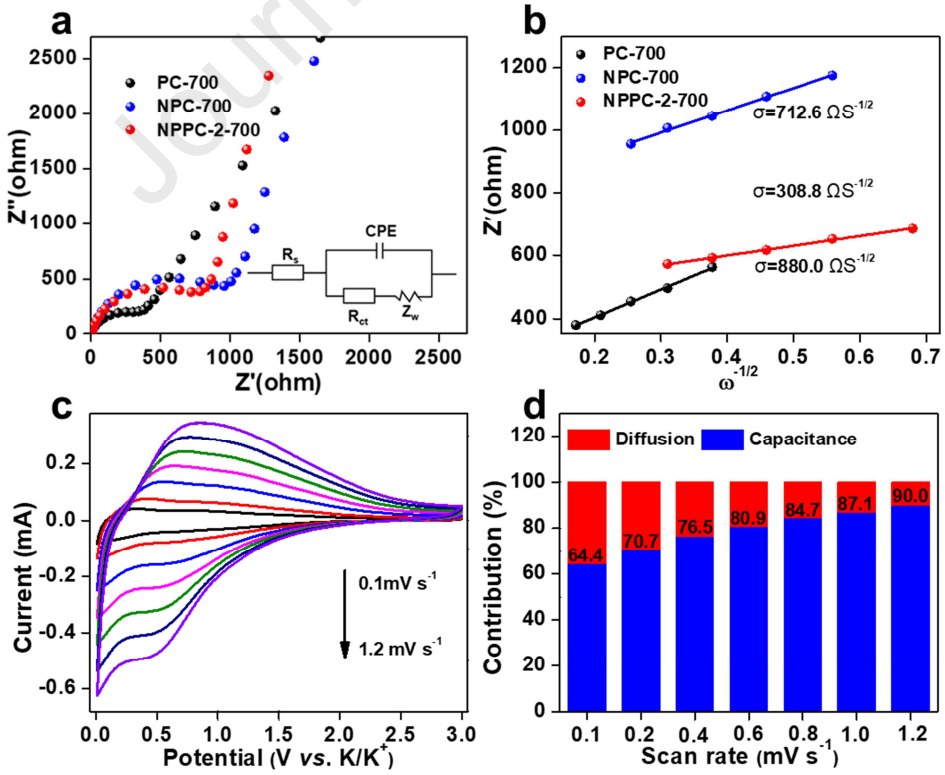

220

Fig. 4. (a) Nyquist plots and (b) the relationship plot between Z' and $\omega^{-1/2}$ at low frequency of Nyquist plots of PC-700, NPC-700 and NPPC-2-700. (c) CV curves at different scan rates and (d) Contribution ratios of capacitive and diffusion capacities at various scan rates of NPPC-2-700.

The σ of samples are shown in Fig. 4b. The K^+ diffusion coefficient (D_k^+) of PC-700, NPC-700 and NPPC-2-700 calculated by equation (1) are 3.02×10^{-14}, 4.60×10^{-14} and 2.45×10^{-13} cm^2 s^{-1}, as shown in Fig. S6a. The D_k^+ of NPPC-2-700 is an order of magnitude higher than that of PC-700, due to the introduction of nitrogen and phosphorus heteroatoms, which expands the carbon interlayer spacing and reduces the potassium ion diffusion resistance. Compared with NPC-700, the co-doping of N and P in NPPC-2-700 cause a drastic distortion of hexagonal carbon skeleton and larger carbon layer spacing, which is more beneficial to increasing the diffusion rate of potassium ions [17].

To further elucidate the mechanism of potassium ion storage, CV measurements were conducted at different scan rates from 0.1 to 1.2 mV s^{-1}. As shown in Fig. 4c, the shape of the CV curves remains well with the increase of scan rates. The relationship of peak current (i) and scan rate (v) is described as the following formula [41]：

$$i = av^b \quad (2)$$

The NPPC-2-700 electrode possesses b values of 0.937 and 0.828 for anodic and cathodic peaks, respectively, indicating the dominant of surface storage process (Fig. S6b). The contribution of surface storage process was calculated from the following equation [42]:

$$i = k_1v^{1/2} + k_2v \quad (3)$$

Where $k_1v^{1/2}$ stands for the diffusion process and k_2v represents the capacitive process. The capacitive contributions of NPPC-2-700 calculated at different scan rates present a similar trend (Figure 4d), i.e., the dominant of capacitive process. At the scan rate of 0.1 mV s^{-1}, the NPPC-2-700 electrode shows a capacitive contribution ratio of 64.4% and reaches 90.0% at scan rate of 1.2 mV s^{-1}. The dominant capacitive storage process of NPPC-2-700 should be attributed to the abundant surface defects and active sites as a result of N and P co-doping. Specifically, P doping is expected to cause more drastic structural distortion of hexagonal carbon skeleton and larger interlayer spacing, which is beneficial to the migration of potassium ions.

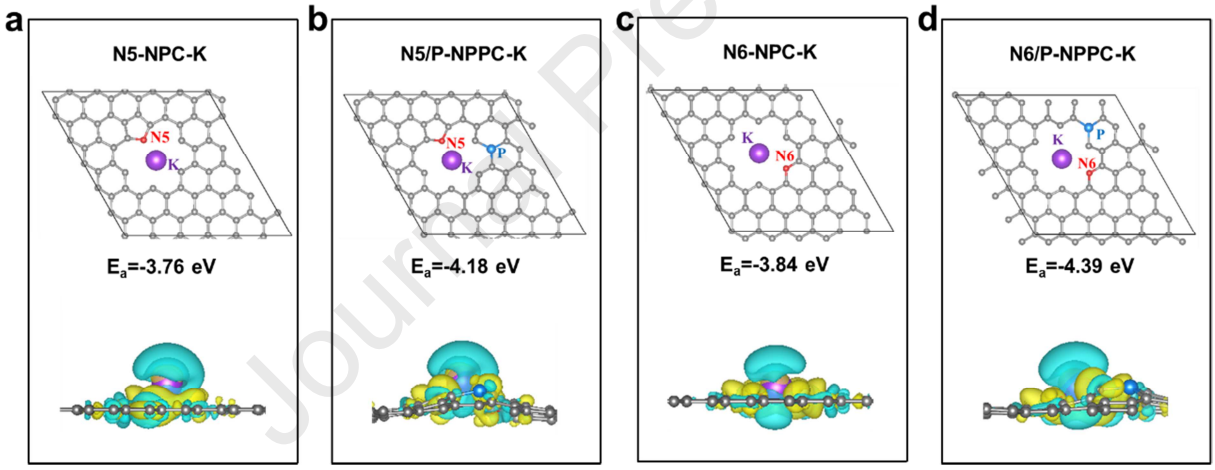

Fig. 5. (a-d) Side view of a single K atom and electron density differences absorbed in N5-NPC-K, N6-NPC-K, N5/P-NPPC-K and N6/P-NPPC-K structures.

In order to investigate the roles of N and P doping on the K adsorption capability, DFT calculations were performed (Fig.5a-d). The adsorption energy (ΔE_a) of N5-NPC-K and N6-NPC-K are -3.76 and -4.18 eV, respectively. After extra P doping, ΔE_a of N5/P-NPPC-K and N6/P-NPPC-K are increased to -3.84 and -4.39 eV, respectively. This phenomenon suggests that N, P co-doped structures has stronger adsorption ability to K^+, which is

consistent with the high rate capability of NPPC. Fig.5a-d show the electron density differences of K adsorbed in the N5-NPC-K, N6-NPC-K, N5/P-NPPC-K and N6/P-NPPC-K structure. The yellow and cyan colors represent the electron accumulation and depletion, respectively. The charge accumulation in NPPC is more obvious than that in NPC, indicating that N/P doping has a stronger adsorption capacity to potassium ions than N doping.

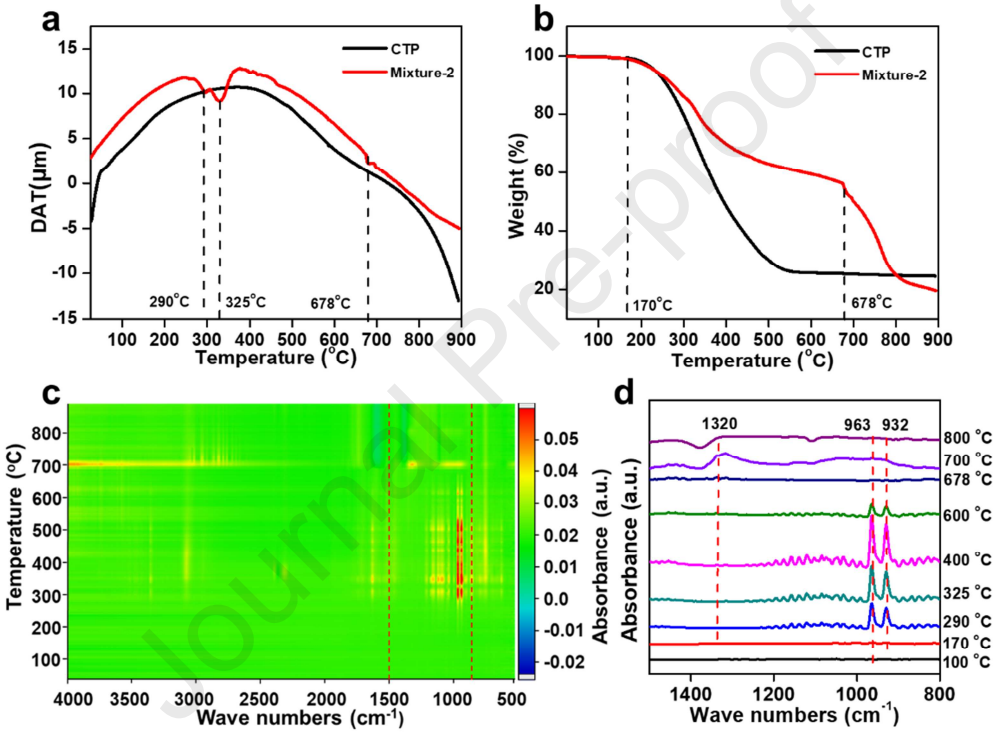

Fig. 6. (a) DTA curves and (b) TG curves of CTP and Mixture-2. (c, d) The in situ FTIR spectra of gas products from raw material for Mixture-2.

To investigate the effect of carbonization temperature on the electrochemical properties of the NPPCs, two control samples with various carbonization temperature of 600 and 800 ^{o}C were prepared. As shown in Fig. S7a, by increasing the calcination temperature, the (002) peak shifts to the higher angle, indicative of the decrease of average interlayer distance. The

I_D/I_G of NPPC-2-600, NPPC-2-700 and NPPC-2-800 are 1.08, 0.99 and 0.88 (Fig. S7b), respectively, indicating the decrease of defect density with raising calcination temperature. Fig. S8a and b exhibit that the P contents are 1.56, 3.15 and 0.32 at.% for NPPC-2-600, NPPC-2-700 and NPPC-2-800, while the contents of N of which are 2.96, 3.68 and 1.79 at.%, indicating that the carbonization temperature is a crucial factor in determining the content of nitrogen and phosphorus.

To investigate the influence of temperature on the N/P doping, TG and DTA of CTP and the mixture of APP and CTP with mass ratios of 2:1, denoted as Mixture-2, were carried out. As shown in Fig. 6a, compared with CTP, DTA curve of the Mixture-2 possesses three extra endothermic peaks. The first two peaks at around 300 ^oC corresponds to the gradual decomposition of APP to produce NH_3 and H_3PO_4. And the third one at 678 ^oC can be attributed to the reaction of H_3PO_4 with carbon. The TG curve of CTP, shown in Fig. 6b, exhibits one-stage weight loss which start from 170 ^oC due to the distillation and pyrolysis of CTP. The carbon yield of CTP is about 30 wt. %. The Mixture-2 exhibits a quite different TG curve with two-stage weight loss, one of which start from 170 ^oC and the other one from 678 ^oC. The first weight loss stage is due to the distillation and pyrolysis of CTP as well as the pyrolysis of APP. While, the second stage is due to the activation of carbon by H_3PO_4, which is accompanied by a drastic weigh loss in the temperature range from 678 to 800 ^oC. The gas products derived from pyrolysis of APP and CTP are analyzed by the in situ FTIR. As shown in Fig. 6c and d, the absorption peaks at 963 and 932 cm^{-1} appeared at 280 ^oC can be ascribed to NH_3, confirming the decomposition of APP. While the peak centered at 1320 cm^{-1} appears from 700 ^oC and disappears at 800 ^oC, implying the reaction of H_3PO_4 with carbon. The

results of TG, DTA and FTIR suggest that the optimal P doping temperature is 700 ^{o}C. The lower temperature results in an insufficient reaction between the carbon and phosphorus, while a higher temperature will lead to a serious loss of the doped phosphorus.

The rate performance of NPPC-2-700 is also better than its counterparts, even at a high current density of 10 A g^{-1}, NPPC-2-700 still retained a reversible capacity of 126 mAh g^{-1}, as shown in Fig. S11a. The cycling stability of NPPCs obtained at different carbonization temperature are shown in Fig. S11b. NPPC-2-700 electrode possesses reversible capacity of 121 mAh g^{-1} after 400 cycles, at current density of 1 A g^{-1}, higher than those of NPPC-2-600 (69 mAh g^{-1}) and NPPC-2-800 (72 mAh g^{-1}). The diffusion coefficient of NPPC-2-700 is larger than others (Fig. S12a and b), due to the high nitrogen and phosphorus contents at the carbonization temperature of 700 ^{o}C.

The effect of the ratio of APP to coal tar pitch on the composition of NPPCs were also investigated. Three samples with different ratio of APP to CTP (1:1, 2:1 and 3:1) were synthesized at 700 □ and recorded as NPPC-1-700, NPPC-2-700 and NPPC-3-700. By increasing the ratio of APP to CTP, the N content of samples increases in the way that was expected, while the P content first increases and then decreases (Fig. 7a and Tab. S1). The correlation between the raw material composition and the content of doped P is not quite clear yet. We speculate that there is some competition between the N doping with NH_3 and P doping with H_3PO_4, or in other words, the P doping is more prone to happening in low-level NH_3 atmosphere. According to the DTA curve (Fig. S9), APP decomposes at about 300-400 ^{o}C and H_3PO_4 react with carbon at 700 ^{o}C. Previous work has reported that the NH_3 can react with pitch at relatively low temperature [34]. As shown in Fig. S10a and b, the in situ FTIR

spectra of gas products from raw material raw material for NPPC-3-700 show the obvious ammonia absorption peaks until 800 ^{o}C, i.e., the H_3PO_4 activation occurred in a high ammonia concentration. In addition, the relative intensity of the 1320 cm^{-1} absorption peak at 700 ^{o}C corresponding to the gas products from H_3PO_4 activation is reduced, suggesting that the H_3PO_4 activation was restrained by high concentration ammonia. Based on the above, the whole reaction can be described as following: firstly, APP decomposes at about 300 ^{o}C to release NH_3 and H_3PO_4. By increasing the temperature, NH_3 is consumed to react with CTP and CTP derived carbon. At 700 ^{o}C, H_3PO_4 activation occurs, which can be significantly affected by the NH_3 concentration, i.e., the high concentration NH_3 restrains the H_3PO_4 activation, which is consistent with the reported work [43].

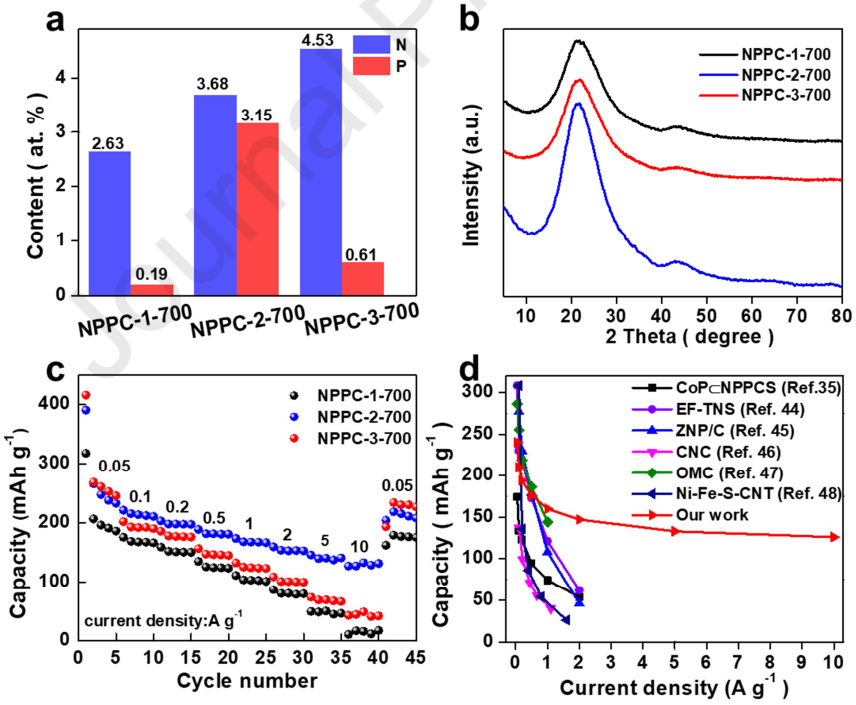

Fig. 7. (a) N and P content, (b) XRD patterns and (c) rate capability at various current densities of NPPCs and (d) Rate performance comparison of NPPC-2-700 with some other reported anode materials.

As shown in the XRD patterns (Fig. 7b) and Raman spectra (Fig. S7b), NPPC-2-700 has the largest interlayer spacing and disorder degree of carbon layer due to the highest P content, which is beneficial for potassium storage. In Fig. 7c and Fig. S11b, as expected, NPPC-2-700 exhibits the highest rate capability and reversible capacity. Thanks to the synergistic effect of the doped nitrogen and phosphorus, the NPPC-2-700 exhibits an excellent rate performance which is superior to the reported PIB anode materials, as shown in Fig. 7d .[35, 44-48]

4 Conclusions

In summary, N and P co-doped coal tar pitch derived porous carbons have been synthesized through a simple one-step carbonization method. The effect of carbonization temperature and the ratio of CTP to APP on the N and P contents were systematically investigated by In situ FTIR and synchronous thermal analysis. The optimal sample (NPPC-2-700) with the highest P content of 3.15% and moderate N content of 3.68% shows good cycling stability (the capacity retention is 81.8 % after 400 cycles) and superior rate performance (126 mAh g^{-1} at 10 A g^{-1}). The excellent potassium storage performance can be mainly ascribed to the synergistic effect of the co-doping N and P as well as the hierarchical porous architecture.

Acknowledgements

This work was supported by the National Natural Science Foundation of China (NSFC, No. U2003216) and the Fundamental Research Funds for the Central Universities of China (No. DUT20LAB131)

References

[1] M. Z. Chen, Q. N. Liu, Z. Hu, Y. Y. Zhang, G. C. Xing, Y. X. Tang, et al., Designing Advanced Vanadium□Based Materials to Achieve Electrochemically Active Multielectron Reactions in Sodium/Potassium□Ion Batteries, Advanced Energy Materials 10(2020), 2002244. https://doi.org/10.1002/aenm.202002244.

[2] D. Kundu, E. Talaie, V. Duffort, L. F. Nazar, The Emerging Chemistry of Sodium Ion Batteries for Electrochemical Energy Storage, Angewandte Chemie International Edition 54(2015), 3431-3448. https://doi.org/10.1002/anie.201410376.

[3] S. Jana, S. Thomas, C. H. Lee, B. Jun, S. U. Lee, Rational design of a PC_3 monolayer: A high-capacity, rapidly charging anode material for sodium-ion batteries, Carbon 157(2020), 420-426. https://doi.org/10.1016/j.carbon.2019.10.086.

[4] J. X. Hu, Y. Y. Xie, M. Yin, Z. A. Zhang, Nitrogen doping and graphitization tuning coupled hard carbon for superior potassium-ion storage, Journal of Energy Chemistry 49(2020), 327-334. https://doi.org/10.1016/j.jechem.2020.03.005.

[5] Y. H. Xie, Y. Chen, L. Liu, P. Tao, M. P. Fan, N. Xu, et al., Ultra-High Pyridinic N-Doped Porous Carbon Monolith Enabling High-Capacity K-Ion Battery Anodes for Both Half-Cell and Full-Cell Applications, Advanced materials 29(2017), 1702268. https://doi.org/10.1002/adma.201702268.

[6] Z. L. Jian, W. Luo, X. L. Ji, Carbon Electrodes for K-Ion Batteries, Journal of the American Chemical Society 137(2015), 11566-115669. https://doi.org/10.1021/jacs.5b06809.

[7] R. Rajagopalan, Y. G. Tang, X. B. Ji, C. K. Jia, H. Y. Wang, Advancements and Challenges in Potassium Ion Batteries: A Comprehensive Review, Advanced Functional Materials 30(2020), 1909486. https://doi.org/10.1002/adfm.201909486.

[8] Y. J. Wu, Y. J. Sun, J. F. Zheng, J. H. Rong, H. Y. Li, L. Niu, MXenes: Advanced materials in potassium ion batteries, Chemical Engineering Journal 404(2021), 126565. https://doi.org/10.1016/j.cej.2020.126565.

[9] S. Thomas, A. K. Madam, M. A. Zaeem, Stone–Wales Defect Induced Performance

Improvement of BC_3 Monolayer for High Capacity Lithium-Ion Rechargeable Battery Anode Applications, The Journal of Physical Chemistry C 124(2020), 5910-5919. https://doi.org/10.1021/acs.jpcc.9b11441.

[10] S. Thomas, C. H. Lee, S. Jana, B. Jun, S. U. Lee, Phographene as a High-Performance Anode Material with High Specific Capacity and Fast Li Diffusion: From Structural, Electronic, and Mechanical Properties to LIB Applications, The Journal of Physical Chemistry C 123(2019), 21345-21352. https://doi.org/10.1021/acs.jpcc.9b04449.

[11] S. Thomas, H. Jung, S. Kim, B. Jun, C. H. Lee, S. U. Lee, Two-dimensional haeckelite h567: A promising high capacity and fast Li diffusion anode material for lithium-ion batteries, Carbon 148(2019), 344-353. https://doi.org/10.1016/j.carbon.2019.03.085.

[12] F. Zhang, P. Xiong, X. Guo, J. Q. Zhang, W. Yang, W. J. Wu, et al., A nitrogen, sulphur dual-doped hierarchical porous carbon with interconnected conductive polyaniline coating for high-performance sodium-selenium batteries, Energy Storage Materials 19(2019), 251-260. https://doi.org/10.1016/j.ensm.2019.03.019.

[13] G. Y. Ma, K. S. Huang, J. S. Ma, Z. C. Ju, Z. Xing, Q. Zhuang, C., Phosphorus and oxygen dual-doped graphene as superior anode material for room-temperature potassium-ion batteries, Journal of Materials Chemistry A 5(2017), 7854-7861. https://doi.org/10.1039/c7ta01108c.

[14] Y. Liu, H. D. Dai, Y. K. An, L. J. Fu, Q. Y. An, Y. P. Wu, Facile and scalable synthesis of a sulfur, selenium and nitrogen co-doped hard carbon anode for high performance Na- and K-ion batteries, Journal of Materials Chemistry A 8(2020), 14993-15001. https://doi.org/10.1039/d0ta04513f.

[15] Q. Sun, D. P. Li, J. Cheng, L. N. Dai, J. G. Guo, Z. Liang, et al., Nitrogen-doped carbon derived from pre-oxidized pitch for surface dominated potassium-ion storage, Carbon 155(2019), 601-610. https://doi.org/10.1016/j.carbon.2019.08.059.

[16] D. P. Li, X. H. Ren, Q. Ai, Q. Sun, L. Zhu, Y. Liu, et al., Facile Fabrication of Nitrogen-Doped Porous Carbon as Superior Anode Material for Potassium-Ion Batteries, Advanced Energy Materials 8(2018), 1802386. https://doi.org/10.1002/aenm.201802386.

[17] X. Ma, G. Ning, C. Qi, C. Xu, J. Gao, Phosphorus and nitrogen dual-doped few-layered

porous graphene: a high-performance anode material for lithium-ion batteries, ACS applied materials & interfaces 6(2014), 14415-14422. https://doi.org/10.1021/am503692g.

[18] Y. T. Luan, R. Hu, Y. Z. Fang, K. Zhu, K. Cheng, J. Yan, et al., Nitrogen and Phosphorus Dual-Doped Multilayer Graphene as Universal Anode for Full Carbon-Based Lithium and Potassium Ion Capacitors, Nano-Micro Letters 11(2019), 30. https://doi.org/10.1007/s40820-019-0260-6.

[19] H. N. He, D. Huang, Y. G. Tang, Q. Wang, X. Ji, B., H. Y. Wang, et al., Tuning nitrogen species in three-dimensional porous carbon via phosphorus doping for ultra-fast potassium storage, Nano Energy 57(2019), 728-736. https://doi.org/10.1016/j.nanoen.2019.01.009.

[20] W. M. Chen, M. Wan, Q. Liu, X. Q. Xiong, F. Q. Yu, Y. H. Huang, Heteroatom□Doped Carbon Materials: Synthesis, Mechanism, and Application for Sodium□Ion Batteries, Small Methods 3(2018), 1800323. https://doi.org/10.1002/smtd.201800323.

[21] H. Q. Li, N. Xiao, M. Y. Hao, X. D. Song, Y. W. Wang, Y. Q. Ji, et al., Efficient CO_2 electroreduction over pyridinic-N active sites highly exposed on wrinkled porous carbon nanosheets, Chemical Engineering Journal 351(2018), 613-621. https://doi.org/10.1016/j.cej.2018.06.077.

[22] G. Kresse, J. Furthmuller, Efficient Iterative Schemes for ab initio Total-Energy Calculations Using a Plane-Wave Basis Set, PHYSICAL REVIEW B 54(1996), 11169-11186. https://doi.org/ 10.1103/PhysRevB.54.11169.

[23] J. P. Perdew, K. Burke, M. Ernzerhof, Generalized Gradient Approximation Made Simple, PHYSICAL REVIEW LETTERS 77(1996), 3865-3868. https://doi.org/10.1103/PhysRevLett.77.3865.

[24] P. E. Blochl, Projector augmented-wave method, Physical review B, Condensed matter 50(1994), 17953-17979. https://doi.org/10.1103/physrevb.50.17953.

[25] S. Grimme, J. Antony, S. Ehrlich, H. Krieg, A Consistent and Accurate ab initio Parametrization of Density Functional Dispersion Correction (DFT-D) for the 94 elements H-Pu, J Chem Phys 132(2010), 154104. https://doi.org/10.1063/1.3382344.

[26] S. Grimme, S. Ehrlich, L. Goerigk, Effect of the damping function in dispersion corrected density functional theory, Journal of computational chemistry 32(2011), 1456-1465. https://doi.org/10.1002/jcc.21759.

[27] P. Lu, Y. Sun, H. Xiang, X. Liang, Y. Yu, 3D Amorphous Carbon with Controlled Porous and Disordered Structures as a High-Rate Anode Material for Sodium-Ion Batteries, Advanced Energy Materials 8(2018), 1702434. https://doi.org/10.1002/aenm.201702434.

[28] Y. W. Wang, N. Xiao, Z. Y. Wang, H. Li, Q., M. L. Yu, Y. C. Tang, et al., Rational design of high-performance sodium-ion battery anode by molecular engineering of coal tar pitch, Chemical Engineering Journal 342(2018), 52-60. https://doi.org/10.1016/j.cej.2018.01.098.

[29] D. C. Qin, Z. Y. Liu, Y. Z. Zhao, G. Y. Xu, F. Zhang, X. G. Zhang, A sustainable route from corn stalks to N, P-dual doping carbon sheets toward high performance sodium-ion batteries anode, Carbon 130(2018), 664-671. https://doi.org/10.1016/j.carbon.2018.01.007.

[30] C. L. Gao, Q. Wang, S. H. Luo, Z. Y. Wang, Y. H. Zhang, Y. G. Liu, et al., High performance potassium-ion battery anode based on biomorphic N-doped carbon derived from walnut septum, Journal of Power Sources 415(2019), 165-171. https://doi.org/10.1016/j.jpowsour.2019.01.073.

[31] W. L. Zhang, J. Yin, M. L. Sun, W. X. Wang, C. L. Chen, M. Altunkaya, et al., Direct Pyrolysis of Supermolecules: An Ultrahigh Edge-Nitrogen Doping Strategy of Carbon Anodes for Potassium-Ion Batteries, Advanced materials 32(2020), 2000732. https://doi.org/10.1002/adma.202000732.

[32] W. D. Qiu, H. B. Xiao, Y. Li, X. H. Lu, Y. X. Tong, Nitrogen and Phosphorus Codoped Vertical Graphene/Carbon Cloth as a Binder-Free Anode for Flexible Advanced Potassium Ion Full Batteries, Small 15(2019), 1901285. https://doi.org/10.1002/smll.201901285.

[33] Y. Qian, S. Jiang, Y. Li, Z. Yi, J. Zhou, T. Q. Li, et al., In Situ Revealing the Electroactivity of P-O and P-C Bonds in Hard Carbon for High□Capacity and Long□Life Li/K□Ion Batteries, Advanced Energy Materials 9(2019), 1901676.

https://doi.org/10.1002/aenm.201901676.

[34] X. Q. Chang, X. L. Zhou, X. W. Ou, C. S. Lee, J. W. Zhou, Y. B. Tang, Ultrahigh Nitrogen Doping of Carbon Nanosheets for High Capacity and Long Cycling Potassium Ion Storage, Advanced Energy Materials 9(2019), 1902672. https://doi.org/10.1002/aenm.201902672.

[35] J. Bai, B. J. Xi, H. Z. Mao, Y. Lin, X. J. Ma, J. K. Feng, et al., One-Step Construction of N,P-Codoped Porous Carbon Sheets/CoP Hybrids with Enhanced Lithium and Potassium Storage, Advanced materials 30(2018), 1802310. https://doi.org/10.1002/adma.201802310.

[36] L. Q. Wang, Z. L. Han, Q. Q. Zhao, X. Y. Yao, Y. Q. Zhu, X. L. Ma, et al., Engineering yolk–shell P-doped NiS_2/C spheres via a MOF-template for high-performance sodium-ion batteries, Journal of Materials Chemistry A 8(2020), 8612-8619. https://doi.org/10.1039/d0ta02568b.

[37] K. Zhang, Q. He, F. Y. Xiong, J. P. Zhou, Y. Zhao, L. Q. Mai, et al., Active sites enriched hard carbon porous nanobelts for stable and high-capacity potassium-ion storage, Nano Energy 77(2020), 105018. https://doi.org/10.1016/j.nanoen.2020.105018.

[38] N. S. Katorova, S. Y. Luchkin, D. P. Rupasov, A. M. Abakumov, K. J. Stevenson, Origins of irreversible capacity loss in hard carbon negative electrodes for potassium-ion batteries, J Chem Phys 152(2020), 194704. https://doi.org/10.1063/5.0003257.

[39] Y. W. Wang, N. Xiao, Z. Y. Wang, Y. C. Tang, H. Q. Li, M. L. Yu, et al., Ultrastable and high-capacity carbon nanofiber anodes derived from pitch/polyacrylonitrile for flexible sodium-ion batteries, Carbon 135(2018), 187-194. https://doi.org/10.1016/j.carbon.2018.04.031.

[40] M. L. Shi, Z. Y. Chen, J. Sun, , Determination of chloride diffusivity in concrete by AC impedance spectroscopy, Cement and Concrete Research 29(1999), 1111-1115. https://doi.org/10.1016/s0008-8846(99)00079-4.

[41] S. T. Liu, B. B. Yang, J. S. Zhou, H. H. Song, Nitrogen-rich carbon-onion-constructed nanosheets: an ultrafast and ultrastable dual anode material for sodium and potassium storage, Journal of Materials Chemistry A 7(2019), 18499-18509.

https://doi.org/10.1039/c9ta04699b.

[42] C. R. Ma, H. J. Yang, Z. X. Xu, Z. G. Fu, Y. Y. Xie, H. T. Zhang, et al., Insights into high capacity and ultrastable carbonaceous anodes for potassium-ion storage via a hierarchical heterostructure, Journal of Materials Chemistry A 8(2020), 2836-2842. https://doi.org/10.1039/c9ta12997a.

[43] C. Yang, J. G. Ren, M. S. Zheng, M. Y. Zhang, Z. Zhong, R. Q. Liu, et al., High-level N/P co-doped Sn-carbon nanofibers with ultrahigh pseudocapacitance for high-energy lithium-ion and sodium-ion capacitors, Electrochimica Acta 359(2020), 136898. https://doi.org/10.1016/j.electacta.2020.136898.

[44] H. J. Tian, X. C. Yu, H. Z. Shao, L. B. Dong, Y. Chen, X. Q. Fang, et al., Unlocking Few□Layered Ternary Chalcogenides for High□Performance Potassium□Ion Storage, Advanced Energy Materials 9(2019), 1901560. https://doi.org/10.1002/aenm.201901560.

[45] C. L. Yan, X. Gu, L. Zhang, Y. Wang, L. T. Yan, D. D. Liu, et al., Highly dispersed Zn nanoparticles confined in a nanoporous carbon network: promising anode materials for sodium and potassium ion batteries, Journal of Materials Chemistry A 6(2018), 17371-17377. https://doi.org/10.1039/c8ta05297b.

[46] B. Cao, Q. Zhang, H. Liu, B. Xu, S. L. Zhang, T. F. Zhou, et al., Graphitic Carbon Nanocage as a Stable and High Power Anode for Potassium-Ion Batteries, Advanced Energy Materials 8(2018), 1801149. https://doi.org/10.1002/aenm.201801149.

[47] W. Wang, J. H. Zhou, Z. P. Wang, L. Y. Zhao, P. H. Li, Y. Yang, et al., Short-Range Order in Mesoporous Carbon Boosts Potassium-Ion Battery Performance, Advanced Energy Materials 8(2018), 1701648. https://doi.org/10.1002/aenm.201701648.

[48] S. P. Zhang, G. Wang, B. B. Wang, J. M. Wang, J. T. Bai, H. Wang, 3D Carbon Nanotube Network Bridged Hetero□Structured Ni□Fe□S Nanocubes toward High□Performance Lithium, Sodium, and Potassium Storage, Advanced Functional Materials 30(2020), 2001592. https://doi.org/10.1002/adfm.202001592.

Highlights

- N and P dual-doped coal tar pitch-based porous carbons was synthesized through a simple one-step carbonization method.
- The effects of carbonation temperature and ratio of ammonium polyphosphate to coal tar pitch on nitrogen and phosphorus doping contents were further investigated by in situ infrared and synchronous thermal analysis.
- The optimal sample with the highest P content of 3.15 % and moderate N content of 3.68 % shows superior rate performance (126 mAh g^{-1} at 10 A g^{-1}).

Conflict of Interest

The authors declare no conflict of interest.